Evidence for a spin phase transition at charge neutrality in bilayer graphene

P. Maher[1], C. R. Dean[2,3], A. F. Young[1], T. Taniguchi[4], K. Watanabe[4], K. L. Shepard[2], J. Hone[3] and P. Kim[1]★

The quantum spin Hall effect is characterized by spin-polarized counter-propagating edge states[1-3]. It has been predicted that this edge state configuration could occur in graphene when spin-split electron- and hole-like Landau levels are forced to cross at the edge of the sample[4-6]. In particular, a quantum-spin-Hall analogue has been predicted in bilayer graphene with a Landau level filling factor $\nu = 0$ if the ground state is a spin ferromagnet[7]. Previous studies have demonstrated that the bilayer $\nu = 0$ state is an insulator in a perpendicular magnetic field[8-14], although the exact nature of this state has not been identified. Here we present measurements of the $\nu = 0$ state in a dual-gated bilayer graphene device in a tilted magnetic field. We map out a full phase diagram of the $\nu = 0$ state as a function of experimentally tunable in-plane magnetic field and perpendicular electric field. At large in-plane magnetic field we observe a quantum phase transition to a metallic state with conductance of the order of $4e^2/h$, consistent with predictions for the ferromagnet.

Under a strong perpendicular magnetic field, bilayer graphene (BLG) develops a $\nu = 0$ quantum Hall state at the charge neutrality point (CNP) that displays anomalous insulating behaviour[8-14]. Transport studies in a dual-gated geometry[10-12] indicate that this gapped state results from an interaction-driven spontaneous symmetry breaking in the valley-spin space[15]. However, the exact order of the resulting ground state remains controversial. In high-mobility suspended BLG devices, a broken-symmetry state at charge neutrality has also been observed at zero magnetic field whose nature has been under intense theoretical[16-22] and experimental[10,12-14,23] investigation. Some experiments indicate there may be a connection between these two insulating states[12,14].

The $\nu = 0$ state in BLG occurs at half-filling of the lowest Landau level. Although the BLG zero-energy Landau level has an additional orbital degeneracy stemming from two accidentally degenerate magnetic oscillator wavefunctions[24], minimization of exchange energy favours singlet pairs in the orbital space at all even filling factors[25]. This leaves an approximate SU(4) spin and pseudospin symmetry for the remaining ordering of the ground state. Comparable ground-state competition has also been studied in double quantum wells in GaAs two-dimensional electron systems[26]. Quantum phase transitions, in particular from canted antiferromagnetic to ferromagnetic ordering, can occur in those systems as an in-plane magnetic field is applied (Zeeman energy is increased)[27,28].

Our experiment is carried out in BLG samples with top and bottom gates in which thin single-crystal hexagonal boron nitride (hBN) serves as a high-quality dielectric on both sides (Fig. 1 bottom inset). By controlling the top gate voltage (V_{TG}) and the
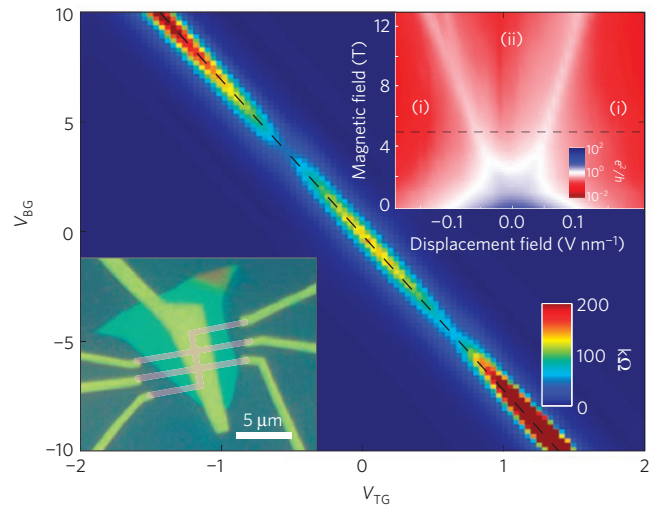

Figure 1 | Device summary. Plot of longitudinal resistance (R_{xx}, colour scale) versus the top gate voltage V_{TG} and the bottom gate voltage V_{BG} at $B_\perp = B_{tot} = 5$ T. The data were taken at 1.5 K. The dashed line indicates the CNP. The top right inset shows four-terminal conductance at the CNP plotted against $B_\perp$ and D. Labels (i) and (ii) indicate the two different insulating $\nu = 0$ phases. The dashed line in the inset corresponds to the dashed line in the main plot. The bottom left inset shows an optical image of the device used in this experiment with false colouring of the graphene (pink).

bottom gate voltage (V_{BG}) we can adjust the carrier density n and the perpendicular electric displacement field D independently. Furthermore, tilting the sample in the magnetic field allows us to independently control the Coulomb energy in a Landau level, e^2/ℓ_B, where the magnetic length ℓ_B is determined by the perpendicular magnetic field $B_\perp$, and Zeeman energy (determined by the total magnetic field B_{tot}). In BLG, B_{tot} and D separately couple to spin and pseudospin, respectively, so our experimental set-up allows us to tune anisotropies and characterize the broken-symmetry quantum Hall states in the approximate SU(4) spin-pseudospin space (see Supplementary Information).

Figure 1 shows the resistance at $B_\perp = B_{tot} = 5$ T measured as a function of the two gate voltages. At zero magnetic field, the resistance at the CNP depends monotonically on $|D|$ owing to the opening of a single particle energy gap[24,29]. With increasing applied magnetic field (Fig. 1 top inset) our device shows the same behaviour reported elsewhere[10-12], with a layer-polarized insulator

[1]Department of Physics, Columbia University, New York, New York 10027, USA, [2]Department of Electrical Engineering, Columbia University, New York, New York 10027, USA, [3]Department of Mechanical Engineering, Columbia University, New York, New York 10027, USA, [4]National Institute for Materials Science, 1-1 Namiki, Tsukuba 305-0044, Japan. *e-mail: pk2015@columbia.edu.
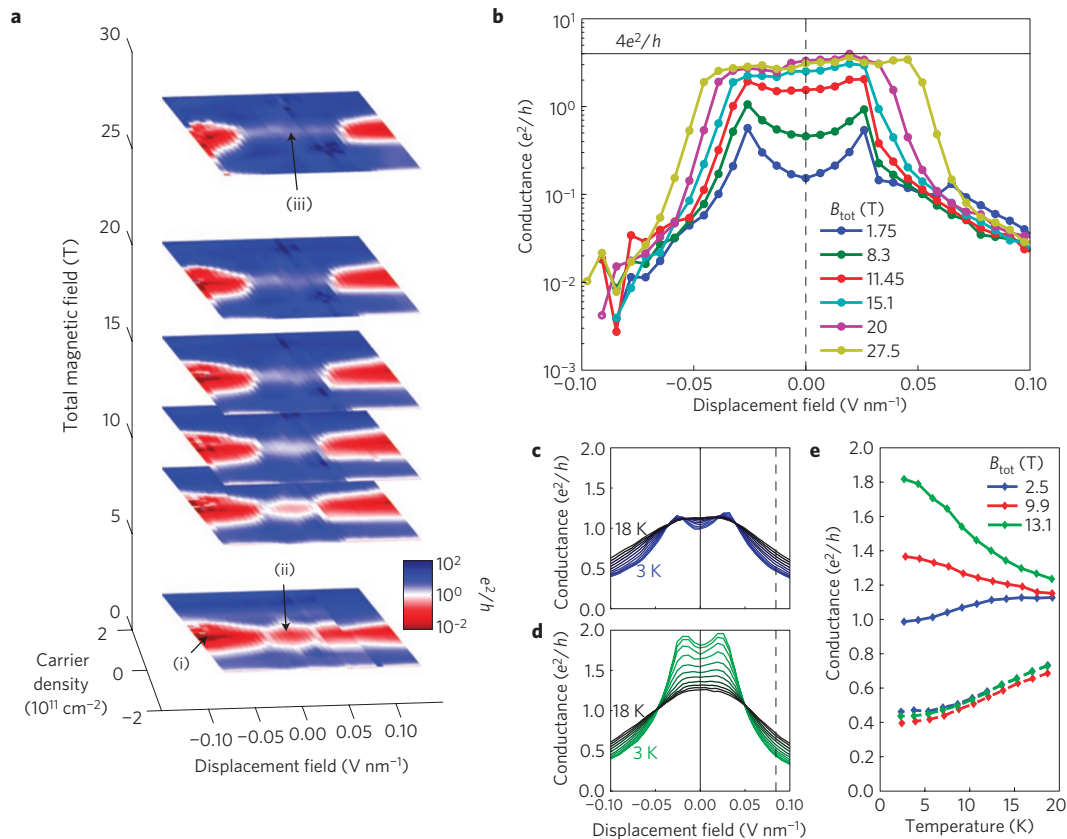
Figure 2 | Tilted-field transport. a, $1/R_{xx}$ plotted against carrier density, displacement field and total magnetic field with $B_{\perp}$ fixed at 1.75 T. Labels (i) and (ii) mark the same phases identified in Fig. 1, and (iii) marks the new conducting phase that appears at large B_{tot}. The data were taken at 350 mK. **b**, Four-terminal conductance at the CNP ($G = 1/R_{xx}$) plotted against displacement field D for a variety of total magnetic fields, $B_{\perp}$ fixed at 1.75 T. The dashed line indicates the zero displacement field points plotted in **c**. The solid line marks the theoretically expected $4e^2/h$ conductance for the ferromagnetic phase. The data were taken at 350 mK. **c,d**, Temperature-dependent four-terminal conductance at the CNP plotted against displacement field, with $B_{\perp} = 2.5$ T, $B_{\mathrm{tot}} = 2.5$ T (**c**), 13.1 T (**d**). The coloured curves were taken at 3 K, black curves at 18 K, and intermediate traces are spaced by 1.5 K. The dashed (solid) vertical lines at a fixed displacement field correspond to the dashed (solid) lines in **e**. **e**, Four-terminal conductance at the CNP for different total magnetic fields plotted against temperature, all at $B_{\perp} = 2.5$ T. The solid lines demonstrate how the behaviour changes as the total field is increased for zero displacement field. The dashed lines demonstrate similar behaviour for all total magnetic fields at $D = 0.085$ V nm^{-1}.

(which we denote phase (i)) observed at large applied displacement field, separated from a low displacement field and high magnetic field quantum Hall insulator (phase (ii)) by a well-defined boundary of finite conductance. Previous studies have reported slopes for this phase boundary in the range of 11–18 mV nm^{-1} T^{-1} (refs 10–12). We obtain values of 7 and 10 mV nm^{-1} T^{-1} for the electron and hole sides, respectively, in reasonable agreement with these previous results. For the remainder of the paper we focus on the behaviour of phase (ii) as we vary the relative Zeeman versus Coulomb energy scales in a rotated field geometry.

Figure 2a shows a series of conductance maps in the vicinity of the CNP. Each pane corresponds to a fixed perpendicular applied magnetic field of 1.75 T, but with varying total field. At a total field of 1.75 T (that is, $B_{\perp} = B_{\mathrm{tot}}$), the distinct insulating regimes at low and high $|D|$ are clearly visible, as discussed in Fig. 1. At low $|D|$ the four-terminal conductance increases markedly with increasing total magnetic field B_{tot}, reaching a value of around 3–4e^2/h, after which it becomes relatively insensitive to either displacement field or magnetic field (Fig. 2b). This rapidly increasing behaviour of conductance at fixed $B_{\perp}$ is consistent with the gradual closing of a gap in phase (ii) as B_{tot} increases. At fixed Coulomb energy, this decreasing gap with increasing Zeeman energy suggests that phase (ii) corresponds to a spin-unpolarized ground state[7–9,13]. In addition, the saturation of conductance at a metallic value around ~4e^2/h at $B_{\mathrm{tot}} \gtrsim 15$ T strongly suggests

a transition into a new phase with a fully closed transport gap, which we label phase (iii).

The transition between insulating and metallic behaviours can further be confirmed by investigating the temperature dependence of the conductance. Figure 2c,d plots four-terminal conductance G at the CNP against D at fixed $B_{\perp} = 2.5$ T with $B_{\mathrm{tot}} = 2.5$ T and 13.1 T, respectively. Temperature T varies between 3 and 18 K. At small $|D|$, G exhibits weakly insulating behaviour for $B_{\mathrm{tot}} = B_{\perp}$ (see Supplementary Information), whereas at $B_{\mathrm{tot}} \gg B_{\perp}$, a metallic temperature dependence (increasing G with decreasing T) is observed. Figure 2e further contrasts the metallic versus insulating classification in different phases by plotting conductance at the CNP against temperature for both large D and $D = 0$. $G(T)$ shows insulating behaviour for phase (ii) ($B_{\perp} \approx B_{\mathrm{tot}}$) and metallic behaviour for phase (iii) ($B_{\perp} \ll B_{\mathrm{tot}}$). At intermediate values of B_{tot} the conductance is relatively temperature insensitive, suggesting a gradual crossover between the two phases. Interestingly, the cusps of high conductance that mark the transition between the layer-polarized and non-layer-polarized phase show a metallic temperature dependence even in a fully perpendicular field. At high D (that is in phase (i)), the conductance remains relatively insensitive to the applied in-plane magnetic field. This is expected for a layer-polarized $\nu = 0$ quantum Hall state, where the energy gap is determined by the applied displacement field.
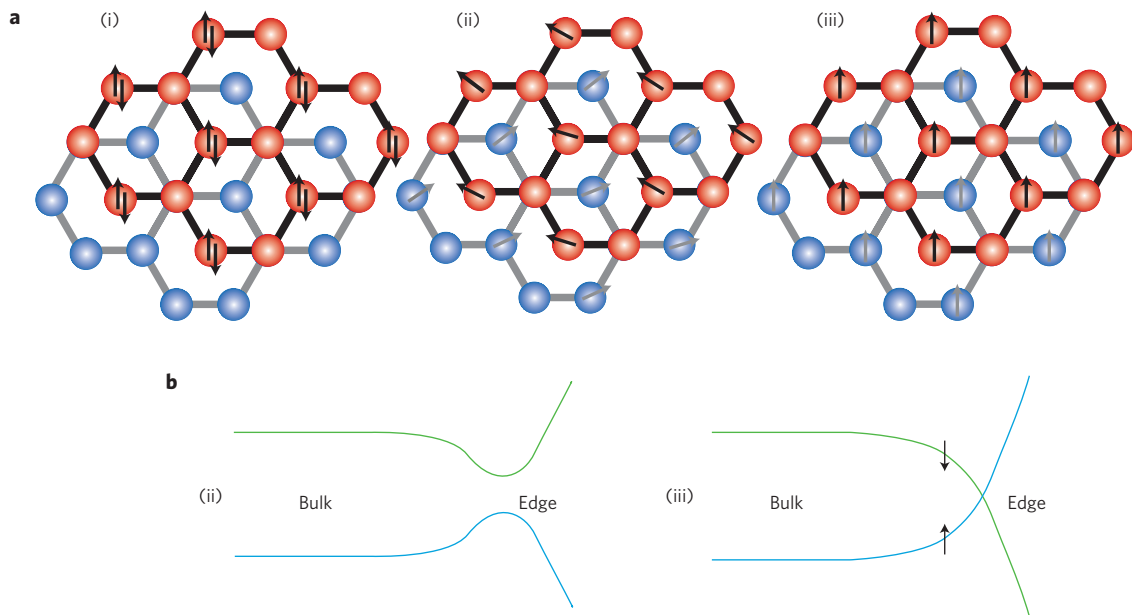
Figure 3 | Candidate states. a, Spin and pseudospin configurations in the BLG $\nu = 0$ state. The illustrations represent the layer-polarized (i), CAF (ii) and ferromagnetic (iii) phases. **b**, Diagram of predicted bulk and edge energy levels for the CAF (ii) and ferromagnetic (iii) phases.

A general theoretical analysis[7] proposes four possible ground states for $\nu = 0$ in BLG: partially layer-polarized (PLP), fully layer-polarized (FLP), canted antiferromagnetic (CAF) or ferromagnetic. Considering that layer pseudospin is synonymous with sublattice and valley pseudospin in the lowest Landau level[24], these four different scenarios can be visualized in terms of spin and sublattice of BLG (Fig. 3a). Which state the system favours depends on both anisotropies in the electron–electron and electron–phonon interactions, and external symmetry-breaking terms such as Zeeman splitting ϵ_Z and interlayer potential energy ϵ_V. The PLP/FLP phases are favoured in the large-ϵ_V limit, and the ferromagnetic phase is favoured in the large-ϵ_Z limit. Unlike in GaAs double wells, these ground states may be accompanied by markedly different transport signatures. The BLG ground-state configurations discussed above are all predicted to be insulators except for the ferromagnetic phase. For the ferromagnetic phase, the highest filled band acquires an electron-like dispersion at the edge whereas the lowest unoccupied band acquires a hole-like dispersion (Fig. 3b; ref. 6). This forces a level crossing at the edge that should result in metallic conductance of $4e^2/h$ due to spin-polarized counter-propagating edge states[4–6]. Interpreting our results in this framework, we can identify phase (i) with either the PLP or FLP state, phase (ii) with the CAF state, and phase (iii) with the ferromagnetic state.

We now focus on the phase diagram of the different ground states classified above. The phase transitions between the layer-polarized, CAF, and ferromagnetic phases can be mapped out by locating the boundary between the metallic ($G \gtrsim e^2/h$) and insulating ($G \ll e^2/h$) regimes as a function of D and B_{tot} with fixed $B_\perp$. For a given B_{tot}, we can define the critical displacement field for transition D^c as the D value that gives maximum change of $\partial G/\partial D$ in $G(D, B_{tot})$ at fixed $B_\perp$. Figure 4a shows the values of D^c and B_{tot} extracted from Fig. 2b ($B_\perp = 1.75$ T). In this D–B_{tot} map three different phases can be identified, corresponding to the layer-polarized, CAF and ferromagnetic phases. Note that the transition between the CAF and layer-polarized phases is sharp, as the conductance changes by an order of magnitude over a D variation $\Delta D \lesssim 0.02$ V nm^{-1}. In contrast the transition from CAF to ferromagnetic is gradual. This observation is consistent with the theoretical expectation that the layer-polarized to CAF or ferromagnetic transition is first order whereas the CAF to

ferromagnetic transition is second order[7]. Further experiments on hysteresis behaviour across the phase boundaries would help to clarify the nature of these phase transitions.

By identifying characteristic energy scales for the external symmetry-breaking terms, we can comment quantitatively on the phase boundaries for a fixed $B_\perp$. We identify Zeeman energy $\epsilon_Z = g\mu_B B_{tot}$, where g and μ_B are the electron spin g-factor and the Bohr magneton respectively, and the interlayer potential energy $\epsilon_V = Dde/2$, where d is the interlayer distance in BLG. For $B_\perp = 1.75$ T, at low B_{tot} the CAF–layer-polarized transition occurs at $\epsilon_V \approx 5$ meV, and at $\epsilon_V = 0$ the CAF–ferromagnet transition occurs at $\epsilon_Z \approx 0.8$ meV. The ferromagnet–layer-polarized transition occurs along a line whose slope $\epsilon_V/\epsilon_Z \approx 2$. The fact that ϵ_V/ϵ_Z at the ferromagnet–layer-polarized phase boundary is of order unity is consistent with the increasing stability of a spin-polarized state with increasing magnetic field, providing further confirmation that the conducting $\nu = 0$ phase is a ferromagnet. This observation is in qualitative agreement with theoretical predictions[7].

At the CNP and $D = 0$, $B_\perp$ is the only physical quantity to control the strength of electron–electron interactions, so the phase boundary between the CAF and ferromagnetic phases can be further investigated by observing G as a function of B_{tot} with different values of fixed $B_\perp$ (see Supplementary Information). Figure 4b shows $G(B_{tot})$ for three different fixed values of $B_\perp$ at $D = 0$. Generally, the behaviour of G can be characterized by two different regimes. For $B_{tot} \sim B_\perp$ (that is, the CAF phase), G increases exponentially as B_{tot} increases. For $B_{tot} \gg B_\perp$ (that is, the ferromagnetic phase), G is insensitive to B_{tot}, saturating close to $4e^2/h$. We define the critical magnetic field B_{tot}^c that separates these two regimes by the intersection of guide lines for the exponential and saturated regimes, as marked by the arrows in Fig. 3b. The identification of B_{tot}^c at different $B_\perp$ allows us to map the phase boundary between the CAF and ferromagnet as a function of $B_\perp$. The inset of Fig. 4b shows B_{tot}^c as a function of $B_\perp$. Although there are only a few data points available to indicate the phase boundary, the general trend of the CAF–ferromagnet phase transition can be inferred from them.

Finally, we remark on the similarity between the ferromagnetic phase of BLG at $\nu = 0$ and the quantum spin Hall effect in HgTe (refs 2,3). In the quantum spin Hall phase, quantized conduction is due to spin-polarized counter-propagating edge states, whereas the
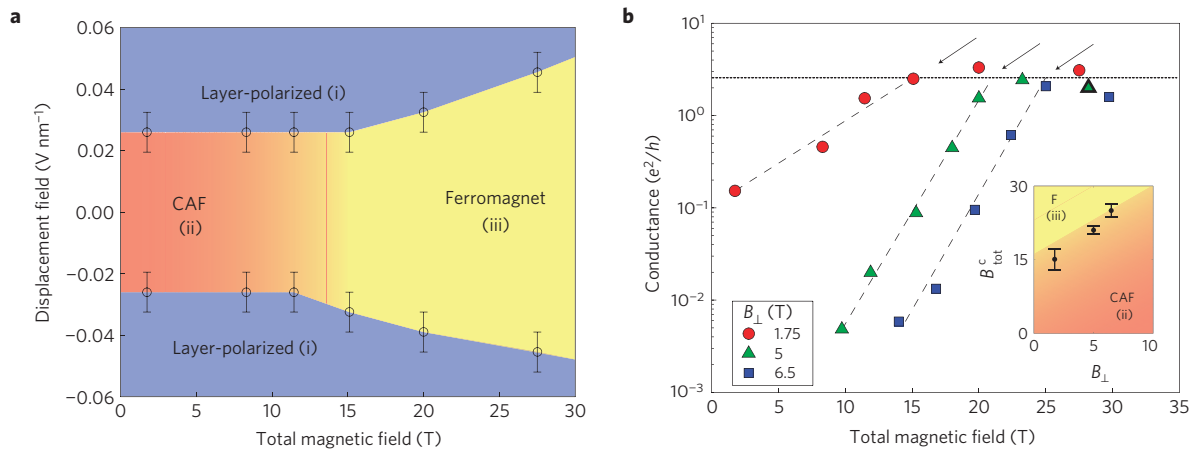
Figure 4 | Phase transitions. a, Different phases of the $\nu = 0$ state mapped as a function of D and B_{tot} at $B_\perp = 1.75$ T. At low B_{tot}, the phase boundary between layer-polarized and CAF is determined by the conductance spike separating the two insulating phases. At large B_{tot}, the phase boundary between layer-polarized and ferromagnetic is determined by the point where conductance begins to exponentially decrease with displacement field. The gradual transition between CAF and ferromagnetic with increasing B_{tot} is marked by the gradual colour change, with ferromagnetic stabilizing at high B_{tot}. Error bars are due to the spacing between adjacent points in D. **b**, Four-terminal conductance at the CNP with $D = 0$, plotted against B_{tot} for three different values of $B_\perp$. Dashed lines indicate regions of exponential increase of conductance and the dotted line marks saturated conductance. The critical magnetic field B_{tot}^c for the phase transition is marked by arrows. The inset shows B_{tot}^c as a function of $B_\perp$ separating the CAF and ferromagnetic phases in a B_{tot} versus $B_\perp$ parameter space. Error bars are due to uncertainties in fitting guide lines.

bulk remains incompressible. An analogous scenario is expected for BLG in the ferromagnetic quantum Hall state[4–6], except that BLG carries an additional orbital degeneracy. The ferromagnetic state in BLG is therefore expected to exhibit a four-terminal conductance of $4e^2/h$, compared with $2e^2/h$ for HgTe. Consistent with reported measurements of HgTe (refs 3,30), our devices show imperfect quantization with measured conductance values less than $4e^2/h$ in the ferromagnetic phase. The reduced conductance may be due to backscattering in the edge state or through remaining impurity states in the bulk. Unambiguous experimental support for the existence of spin-polarized counter-propagating edge states should be provided by well-quantized nonlocal measurements[30] (see Supplementary Information).

We have measured dual-gated graphene bilayers at the $\nu = 0$ state. In a perpendicular magnetic field, we observe a transition between two incompressible states at a finite displacement field, indicating that the $D = 0$ state is not layer polarized. At low displacement fields, we observe the four-terminal conductance increase and then saturate as the in-plane magnetic field increases, showing that the $D = 0$, $B_{tot} = B_\perp$ state is also not spin polarized. This is consistent with a quantum phase transition driven by in-plane magnetic field between the CAF quantum Hall state and the ferromagnet. The near quantization of the four-terminal conductance to $4e^2/h$ agrees with predictions that the ferromagnetic quantum Hall ground state carries spin-polarized counter-propagating edge states.

Methods

The device we report data from was fabricated with mechanically exfoliated graphene and hBN using a polymer membrane transfer process described in previous work[31]. The graphene was etched into a Hall bar pattern before deposition of the top hBN layer. The bottom gate is a global silicon gate, and both the contacts and the top gate are Cr/Pd/Au stacks of thickness 1/10/50 nm. Three devices fabricated in a similar way exhibited similar data trends, although the phase boundaries may be quantitatively sample- and disorder-dependent (see Supplementary Information). We present data sets obtained from the highest quality device.

These devices were measured either in a sample-in-^{4}He-vapour variable temperature cryostat with a 14 T magnet in-house or in a sample-in-^{3}He-vapour cryostat, mounted in the bore of a 31 T resistive magnet at the National High Magnetic Field Laboratory in Tallahassee, Florida. Measurements were performed using a 1 mV voltage bias. The numerous features present in a gate voltage trace allowed precise angle calibration, with $B_\perp$ determined to better than 1% accuracy. The longitudinal resistance R_{xx} and Hall resistance R_{xy} are measured in a

four-terminal geometry, so that contact resistances can be excluded. Four-terminal conductance at the CNP is obtained by taking $G = 1/R_{xx}$.

References

1. Kane, C. L. & Mele, E. J. Z_2 topological order and the quantum spin Hall effect. *Phys. Rev. Lett.* **95,** 146802 (2005).
2. Bernevig, B. A., Hughes, T. L. & Zhang, S-C. Quantum spin Hall effect and topological phase transition in HgTe quantum wells. *Science* **314,** 1757–1761 (2006).
3. König, M. *et al.* Quantum spin Hall insulator state in HgTe quantum wells. *Science* **318,** 766–770 (2007).
4. Abanin, D. A., Lee, P. A. & Levitov, L. S. Spin-filtered edge states and quantum Hall effect in graphene. *Phys. Rev. Lett.* **96,** 176803 (2006).
5. Fertig, H. A. & Brey, L. Luttinger liquid at the edge of undoped graphene in a strong magnetic field. *Phys. Rev. Lett.* **97,** 116805 (2006).
6. Kharitonov, M. Edge excitations of the canted antiferromagnetic phase of the $\nu = 0$ quantum Hall state in graphene: A simplified analysis. *Phys. Rev. B* **86,** 075450 (2012).
7. Kharitonov, M. Canted antiferromagnetic phase of the $\nu = 0$ quantum Hall state in bilayer graphene. *Phys. Rev. Lett.* **109,** 046803 (2012).
8. Feldman, B. E., Martin, J. & Yacoby, A. Broken-symmetry states and divergent resistance in suspended bilayer graphene. *Nature Phys.* **5,** 889–893 (2009).
9. Zhao, Y., Cadden-Zimansky, P., Jiang, Z. & Kim, P. Symmetry breaking in the zero-energy Landau level in bilayer graphene. *Phys. Rev. Lett.* **104,** 066801 (2010).
10. Weitz, R. T., Allen, M. T., Feldman, B. E., Martin, J. & Yacoby, A. Broken-symmetry states in doubly gated suspended bilayer graphene. *Science* **330,** 812–816 (2010).
11. Kim, S., Lee, K. & Tutuc, E. Spin-polarized to valley-polarized transition in graphene bilayers at $\nu = 0$ in high magnetic fields. *Phys. Rev. Lett.* **107,** 016803 (2011).
12. Velasco, J. Jr *et al.* Transport spectroscopy of symmetry-broken insulating states in bilayer graphene. *Nature Nanotech.* **7,** 156–160 (2012).
13. Veligura, A. *et al.* Transport gap in suspended bilayer graphene at zero magnetic field. *Phys. Rev. B* **85,** 155412 (2012).
14. Freitag, F., Trbovic, J., Weiss, M. & Schenberger, C. Spontaneously gapped ground state in suspended bilayer graphene. *Phys. Rev. Lett.* **108,** 076602 (2012).
15. Gorbar, E. V., Gusynin, V. P. & Miransky, V. A. Dynamics and phase diagram of the $\nu = 0$ quantum Hall state in bilayer graphene. *Phys. Rev. B* **81,** 155451 (2010).
16. Lemonik, Y., Aleiner, I. L. & Falko, V. I. Competing nematic, antiferromagnetic, and spin-flux orders in the ground state of bilayer graphene. *Phys. Rev. B* **85,** 245451 (2012).

17. Kharitonov, M. Antiferromagnetic state in bilayer graphene. *Phys. Rev. B* **86,** 195435 (2012).
18. Zhang, F. & MacDonald, A. H. Distinguishing spontaneous quantum Hall states in bilayer graphene. *Phys. Rev. Lett.* **108,** 186804 (2012).
19. Lemonik, Y., Aleiner, I. L., Toke, C. & Falko, V. I. Spontaneous symmetry breaking and Lifshitz transition in bilayer graphene. *Phys. Rev. B* **82,** 201408 (2010).
20. Vafek, O. & Yang, K. Many-body instability of Coulomb interacting bilayer graphene: Renormalization group approach. *Phys. Rev. B* **81,** 041401 (2010).
21. Nandkishore, R. & Levitov, L. Quantum anomalous Hall state in bilayer graphene. *Phys. Rev. B* **82,** 115124 (2010).
22. Castro, E. V., Peres, N. M. R., Stauber, T. & Silva, N. A. P. Low-density ferromagnetism in biased bilayer graphene. *Phys. Rev. Lett.* **100,** 186803 (2008).
23. Mayorov, A. S. *et al.* Interaction-driven spectrum reconstruction in bilayer graphene. *Science* **333,** 860–863 (2011).
24. McCann, E. & Falko, V. I. Landau-level degeneracy and quantum Hall effect in a graphite bilayer. *Phys. Rev. Lett.* **96,** 086805 (2006).
25. Barlas, Y., Ct, R., Nomura, K. & MacDonald, A. H. Intra-Landau-level cyclotron resonance in bilayer graphene. *Phys. Rev. Lett.* **101,** 097601 (2008).
26. Das Sarma, S., Sachdev, S. & Zheng, L. Double-layer quantum Hall antiferromagnetism at filling fraction $\nu = 2/m$ where m is an odd integer. *Phys. Rev. Lett.* **79,** 917–920 (1997).
27. Pellegrini, V. *et al.* Evidence of soft-mode quantum phase transitions in electron double layers. *Science* **281,** 799–802 (1998).
28. Grivei, E., Melinte, S., Bayot, V., Manoharan, H. C. & Shayegan, M. Multiple interacting bilayer electron system: Magnetotransport and heat capacity measurements. *Phys. Rev. B* **68,** 193404 (2003).
29. Taychatanapat, T. & Jarillo-Herrero, P. Electronic transport in dual-gated bilayer graphene at large displacement fields. *Phys. Rev. Lett.* **105,** 166601 (2010).
30. Roth, A. *et al.* Nonlocal transport in the quantum spin Hall state. *Science* **325,** 294–297 (2009).
31. Dean, C. R. *et al.* Boron nitride substrates for high-quality graphene electronics. *Nature Nanotech.* **5,** 722–726 (2010).

Acknowledgements

Author contributions

P.M., C.R.D. and A.F.Y. designed and conceived the experiment. T.T. and K.W. synthesized hBN samples, P.M. fabricated the samples. P.M., C.R.D. and A.F.Y. performed the measurements. P.M., C.R.D. and P.K. analysed the data and wrote the paper. J.H., K.L.S. and P.K. advised on experiments.

Additional information

Supplementary information is available in the online version of the paper. Reprints and permissions information is available online at www.nature.com/reprints. Correspondence and requests for materials should be addressed to P.K.

Competing financial interests

The authors declare no competing financial interests.